Immunity, Volume *50*

Supplemental Information

Cell-Type-Specific Interleukin 1 Receptor 1 Signaling in the Brain Regulates Distinct Neuroimmune Activities

Xiaoyu Liu, Daniel P. Nemeth, Daniel B. McKim, Ling Zhu, Damon J. DiSabato, Olimpia Berdysz, Gowthami Gorantla, Braedan Oliver, Kristina G. Witcher, Yufen Wang, Christina E. Negray, Rekha S. Vegesna, John F. Sheridan, Jonathan P. Godbout, Matthew J. Robson, Randy D. Blakely, Phillip G. Popovich, Staci D. Bilbo, and Ning Quan

Figure S1. Examination of IL-1R1 mRNA and Cre expression in cell-type specific Cre and IL-1R1 lines. Related to Figure 1 and Figure 2.

(A-B) Results of ISHH labeling of brain sections from WT (A) and *Il1r1*$^{r/r}$ mice (B). IL-1R1 riboprobe labeling was found in the endothelial cells (A, left), choroid plexus cells (A, middle) and ependymal cells (A, right) in the WT mice and was absent in the dentate gyrus (B, left), choroid plexus cells (B, middle) and endothelial cells (B, right) in the *Il1r1*$^{r/r}$ mice. Scale bar: 100 μm. Dashed square marks the area shown at higher magnification on the bottom right.

(C) IHC labeling of DAPI, RFP and CD31 of hippocampal sections from WT mice. Scale bar: 100 μm. RFP is not present in these mice without the knockin tdTomato.

(D-F) IHC labeling of the reporter for *Tie2*-Cre (D, middle), *Cx3xr1*-Cre (E, middle), and *Gfap*-Cre (F, middle) with cell-type specific markers Ly6C (D, left), Iba1 (E, left) and GFAP (F, left) of brain sections from *Tie2*-Cre-R26tdT, *Cx3cr1*-Cre-R26tdT and *Gfap*-Cre-R26tdT mice. Scale bar for (D-E): 100 μm. Scale bar for (F): 50 μm.

(G-H) Representative tilescan images of tdTomato (G) and eGFP (H) labeling of hippocampus sections from *Camk2a*-Cre-R26tdT and *Vglut2*-Cre-R26tdT mice. Scale bar: 200 μm.

(I) IHC labeling of NeuN and RFP of brain sections from *Gfap*-Cre-*Il1r1*$^{r/r}$ mice. Scale bar: 100 μm.

(J) Representative tilescan images of RFP labeling of *Vglut2*-Cre-*Il1r1*$^{r/r}$ hippocampal sections. Scale bar: 200 μm.

(K-L) Representative images of RFP labeling of brain sections from *Gfap*-Cre-*Il1r1*$^{r/r}$ mice after sham/IL-1 injections. Scale bar: 50 μm.

(M) IHC labeling of Iba1 and RFP of hippocampal sections from *Cx3cr1*-Cre-*Il1r1*$^{r/r}$ mice. Scale bar: 100 μm.

(N) IHC labeling of RFP, PDGFRβ and CD31 of brain sections from *Tie2*-Cre-*Il1r1*$^{r/r}$ mice. Arrow indicates a PDGFRβ-labeled pericyte cell body. Dashed square marks the area shown for RFP and CD31 co-localization (top right) or RFP and PDGFRβ (bottom right) double labeled images at higher magnification. Scale bar: 25 μm.

(O) qPCR analysis of inflammatory genes in hippocampus samples of WT and *Tie2*-Cre-*Il1r1*$^{r/r}$COX-2$^{f/f}$ mice following ICV sham/IL-1β injections. n = 4 mice/genotype, 3 independent experiments.

Error bars represent the mean ± SEM. Means with asterisk (*) are significantly different from the corresponding control group ($p < 0.05$) according to *F*-protected post hoc analysis.

Figure S2. eIL-1R1 and nIL-1R1 cause distinct neuroinflammatory responses. Related to Figure 3.

(A) Representative images of CD45 and Iba1 labeling on injection side of DG sections from WT, *Il1r1*$^{r/r}$, *Tie2*-Cre-*Il1r1*$^{r/r}$ and V*glut2*-Cre-*Il1r1*$^{r/r}$ mice 6 days after high dose ad-ssIL-1 injections. Dashed square marks the area shown at higher magnification on the bottom right. Scale bar: 100 μm.

(B-C) Quantification of Iba1 proportional area (B) and CD45^{+} cells (C) on injection side and contralateral side of DG sections from WT, *Il1r1*$^{r/r}$, *Tie2*-Cre-*Il1r1*$^{r/r}$ and V*glut2*-Cre-*Il1r1*$^{r/r}$ mice 6 days after ad-ssIL-1 injections. n = 4 mice/genotype, 2 independent experiments.

(D) Representative images of CD45 and Iba1 labeling on injection side of DG sections from WT, *Il1r1*$^{r/r}$, *Tie2*-Cre-*Il1r1*$^{r/r}$ and V*glut2*-Cre-*Il1r1*$^{r/r}$ mice 6 days after low dose ad-ssIL-1 injections. Dashed square marks the area shown at higher magnification on the bottom right. Scale bar: 100 μm.

(E) Quantification of Iba1 proportional area on injection side and contralateral side of DG sections from WT, *Il1r1*$^{r/r}$, *Tie2*-Cre-*Il1r1*$^{r/r}$ and V*glut2*-Cre-*Il1r1*$^{r/r}$ mice 6 days after ad-ssIL-1 injections. n = 4 mice/genotype, 2 independent experiments.

Error bars represent the mean ± SEM. Means with asterisk (*) are significantly different from the corresponding control group ($p < 0.05$) according to *F*-protected post hoc analysis.

Figure S3. Microglial activation and leukocyte recruitment occur independently in response to IL-1. Related to Figures 4-6.
(A-E) Influence of leukocyte depletion by vinblastine/cyclophosphamide on central IL-1 induced microglial morphological alterations. (F-H) Influence of microglia depletion by PLX on central IL-1 induced leukocyte recruitment.
(A) Representative images of CD45 and Iba1 labeling of hippocampus sections from saline, vinblastine or cyclophosphamide treated WT mice 24 h after ICV IL-1β injections. Scale bar: 100 µm.
(B-D) Quantification of Iba1 proportional area (B), average microglial total process length (C), and microglial soma size (D) in DG sections from saline, vinblastine or cyclophosphamide treated WT mice 24 h after ICV IL-1β injections. n = 4-5 mice/genotype, 3 independent experiments.
(E) Quantification of parenchymal $CD45^+$ cell number in the DG sections from saline, vinblastine or cyclophosphamide treated WT mice 24 h after ICV IL-1β injections. n = 4 mice/group, 3 independent experiments.
(F) Quantification of parenchymal $Iba1^+$ cell number in brain sections from PLX treated WT mice after ICV IL-1β injections. n = 4 mice/group, 2 independent experiments.
(G) Cell counts of microglia and infiltrating leukocytes in the brain by FACS analyses. n = 3 mice/group, 2 independent experiments.
(H) Representative images of CD45 and Iba1 labeling of brain sections from PLX treated WT mice 24 h after ICV sham/IL-1β injection. Scale bar: 100 µm.
Error bars represent the mean ± SEM. Means with asterisk (*) are significantly different from the corresponding control group ($p < 0.05$) according to *F*-protected post hoc analysis. Vinbl, vinblastine; Cyclo, cyclophosphamide.

Figure S4. Influence of depletion of circulating leukocytes on microglial morphology and influence of depletion of brain microglia on leukocyte trafficking. Related to Figures 4-6.
(A) Representative flow bivariate dot plots of CD11b, Ly6C and Ly6G labeling on enriched blood monocytes and neutrophils from saline, vinblastine or cyclophosphamide treated WT mice.
(B) Cell counts of total leukocytes, $CD11b^+Ly6G^+Ly6C^{int}$ neutrophils and $CD11b^+Ly6G^-Ly6C^{hi}$ monocytes in the blood from saline, vinblastine or cyclophosphamide treated WT mice. n = 4 mice/group, 4 independent experiments.
(C) Representative images of CD45 and Iba1 labeling of the hippocampus sections from saline, vinblastine or cyclophosphamide treated mice which received sham injections. Scale bar: 100 µm.
(D-E) Quantification of Iba1 proportional area of medial orbital cortex (D) and septal area (E) sections from saline, vinblastine or cyclophosphamide treated WT mice which received sham/IL-1β injections. n = 4 mice/group, 3 independent experiments.
(F) Cell counts of whole brain monocytes, lymphocytes and neutrophils by flow cytometry in PLX or control diet treated WT mice after saline or LPS injections. n = 6-8 mice/group. SAL, saline, 2 independent experiments.
Error bars represent the mean ± SEM. Means with asterisk (*) are significantly different from the corresponding control group ($p < 0.05$) according to *F*-protected post hoc analysis.

Figure S5. Mechanistic study of central IL-1 induced leukocyte infiltration. Related to Figure 4.
(A) Schematic of the generation of *Il1r1*$^{r/r}$ bone marrow chimera (BM$^{Il1r1r/r \rightarrow Il1r1r/r}$ and BM$^{Il1r1r/r \rightarrow Tie2\text{-}Cre\text{-}Il1r1r/r)}$ mice.

(B) IHC labeling of Iba1 and CD45 of brain sections from BM$^{Il1r1r/r \rightarrow Il1r1r/r}$ and BM$^{Il1r1r/r \rightarrow Tie2\text{-Cre-}Il1r1r/r}$ mice 24 h after ICV IL-1β injections. Dashed square marks the area shown at higher magnification on the top left. Scale bar: 50 μm.
(C) Ratio of infiltrating CD11b^{+}CD45^{+} leukocytes relative to numbers of microglia in whole brains from BM$^{Il1r1r/r \rightarrow Il1r1r/r}$ and BM$^{Il1r1r/r \rightarrow Tie2\text{-Cre-}Il1r1r/r}$ mice. n = 4 mice/genotype, 2 independent experiments.
(D) IHC labeling of CD45 and CD31 of hippocampal sections from ICV IL-1β injected WT, *Tie2*-Cre-*Il1r1*$^{r/r}$ and *Tie2*-Cre-*Il1r1*$^{f/f}$ mice. Scale bar: 100 μm.
(E) IHC labeling of RFP, GFAP, Iba1, CD31 and CD206 of brain sections from CCL2RFP^{flox} mice after ICV sham/IL-1β injections. Dashed square marks the area shown at higher magnification on the bottom right. An orthogonal view of each higher magnification, double-labeled, z-stack image is presented on the far right. White lines represent vertical or horizontal optical cuts through the stack. Scale bar for top three panels: 100 μm. Scale bar for bottom three panels: 50 μm.
(F) Relative CCL2 mRNA levels of brain tissues from WT mice after PLX treatment and the rest mouse lines 3 h following ICV IL-1β injections, complementary to IL-1R1 lines shown in Figure 5F. n = 4-5 mice/genotype, 3 independent experiments.
Error bars represent the mean ± SEM. Means with different letters (a, b, c, d) show groups that are significantly different ($p < 0.05$) according to *F*-protected post hoc analysis.

Figure S6. Central IL-1 induces CAM expression in IL-1R1^{+}/IL-1R1^{-} endothelial and ependymal cells. Related to Figure 5.
(A-B) IHC labeling of RFP (A-B), ICAM-1 (A) and VCAM-1 (B) of brain sections from *Il1r1*$^{GR/GR}$ mice after ICV IL-1β injections. Scale bar: 100 μm.
(C) Quantification of RFP and ICAM/VCAM colocalization of brain sections from *Il1r1*$^{GR/GR}$ mice after ICV IL-1β injections. n = 3 mice/group, 2 independent experiments.
(D-E) Representative tilescan images of VCAM-1 (D) and ICAM-1 (E) labeling of brain sections from WT, *Tie2*-Cre-*Il1r1*$^{r/r}$ and *Tie2*-Cre-*Il1r1*$^{f/f}$ mice after sham/IL-1β injections. Arrows point to ICAM expression in ependymal cells at the lateral ventricle. Scale bar: 200 μm.

Figure S7. Cell-type specific IL-1R1s mediate changes in microglial morphology and gene expressions. Related to Figure 6.
(A-B) Quantification of average microglial total process length (A) and Iba1^{+} cell density (B) of DG sections from cell-type specific IL-1R1 lines 24 h after ICV IL-1β injections. n = 4-5 mice/genotype, 5 independent experiments.
(C) qPCR analysis of NOS2 in hippocampus samples of cell-type specific IL-1R1 lines and PLX treated WT mice 3 h following ICV sham/IL-1β injections. n = 4-5 mice/genotype, 6 independent experiments.
(D) qPCR analysis of inflammatory genes in of *Il1r1*$^{f/f}$, *Tie2*-Cre-*Il1r1*$^{f/f}$ and *Gfap*-Cre-*Il1r1*$^{f/f}$ mice 3 h following ICV sham/IL-1β injections. n = 4 mice/genotype, 4 independent experiments.
(E) IHC labeling of RFP and GFAP of striatum sections from ICV IL-1β injected AAVCre-*Il1r1*$^{r/r}$ mice. Dashed square marks the area shown at higher magnification on the bottom. Scale bar: 100 μm.
(F) IL-6 mRNA levels of sham injected, control side (AAVGFP) and aIL-1R1 KO side (AAVCre) striatum in AAVCre-*Il1r1*$^{f/f}$ mice. n = 4-5 mice/genotype, 1 independent experiment.
(G-H) Quantification of mean fluorescence intensity (MFI) of CD86 (G) and CD11b (H) in microglia from ICV IL-1β injected WT, *Tie2*-Cre-*Il1r1*$^{r/r}$ and *Tie2*-Cre-*Il1r1*$^{f/f}$ mice by flow cytometric analysis. n = 4 mice/per genotype, 4 independent experiments.
Error bars represent the mean ± SEM. Means with different letters (a, b, c, d) or means with asterisk (*) show groups that are significantly different ($p < 0.05$) according to *F*-protected post hoc analysis.

Figure S1

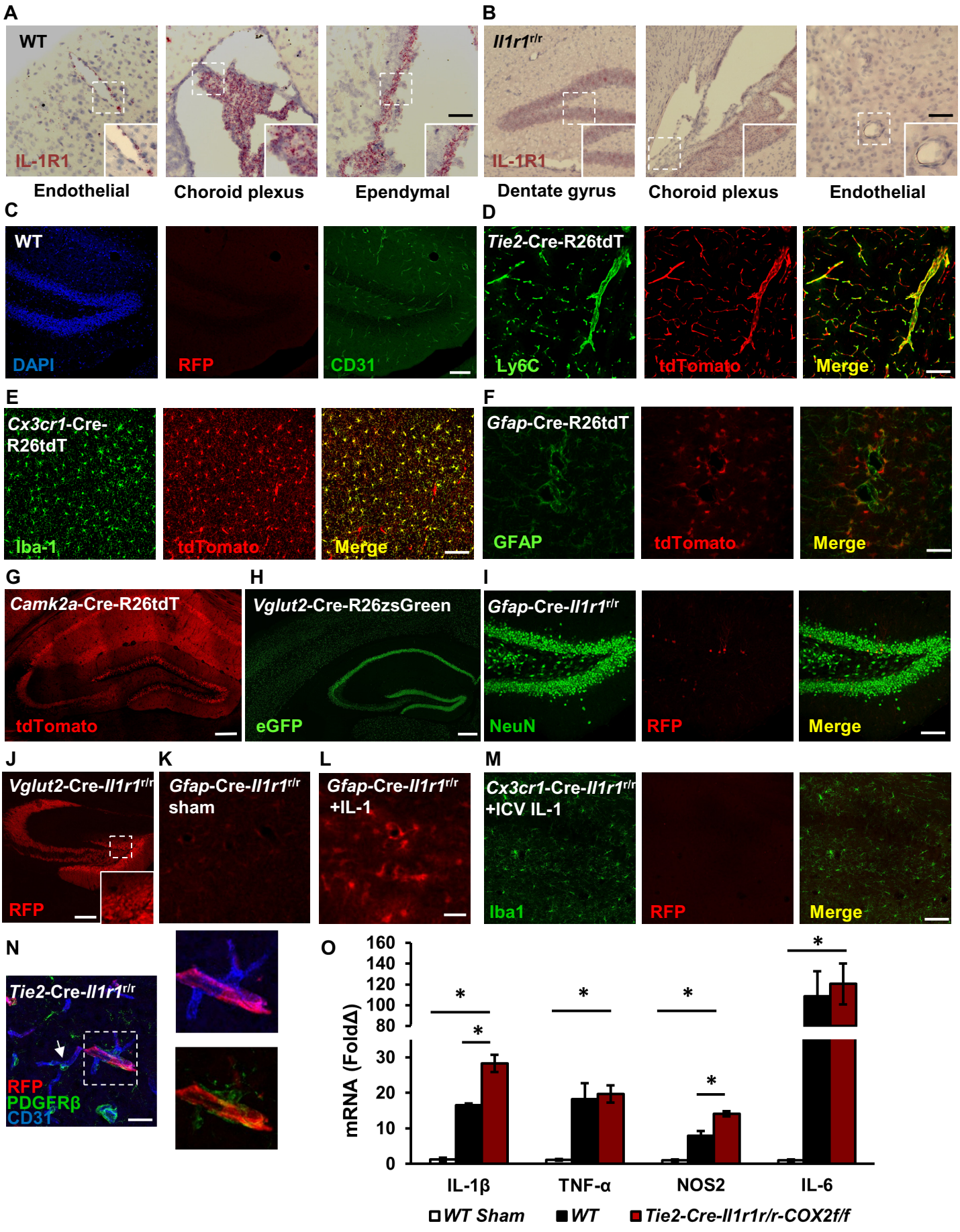
A
WT
IL-1R1
Endothelial
Choroid plexus
Ependymal
B
Il1r1r/r
IL-1R1
Dentate gyrus
Choroid plexus
Endothelial
C
WT
DAPI
RFP
CD31
D
Tie2-Cre-R26tdT
Ly6C
tdTomato
Merge
E
Cx3cr1-Cre-R26tdT
Iba-1
tdTomato
Merge
F
Gfap-Cre-R26tdT
GFAP
tdTomato
Merge
G
Camk2a-Cre-R26tdT
tdTomato
H
Vglut2-Cre-R26zsGreen
eGFP
I
Gfap-Cre-Il1r1r/r
NeuN
RFP
Merge
J
Vglut2-Cre-Il1r1r/r
RFP
K
Gfap-Cre-Il1r1r/r
sham
L
Gfap-Cre-Il1r1r/r
+IL-1
M
Cx3cr1-Cre-Il1r1r/r
+ICV IL-1
Iba1
RFP
Merge
N
Tie2-Cre-Il1r1r/r
RFP
PDGFRβ
CD31
O
mRNA (FoldΔ)
160
140
120
100
80
30
20
10
0
*
IL-1β
TNF-α
NOS2
IL-6
WT Sham
WT
Tie2-Cre-Il1r1r/r-COX2f/f

Figure S2

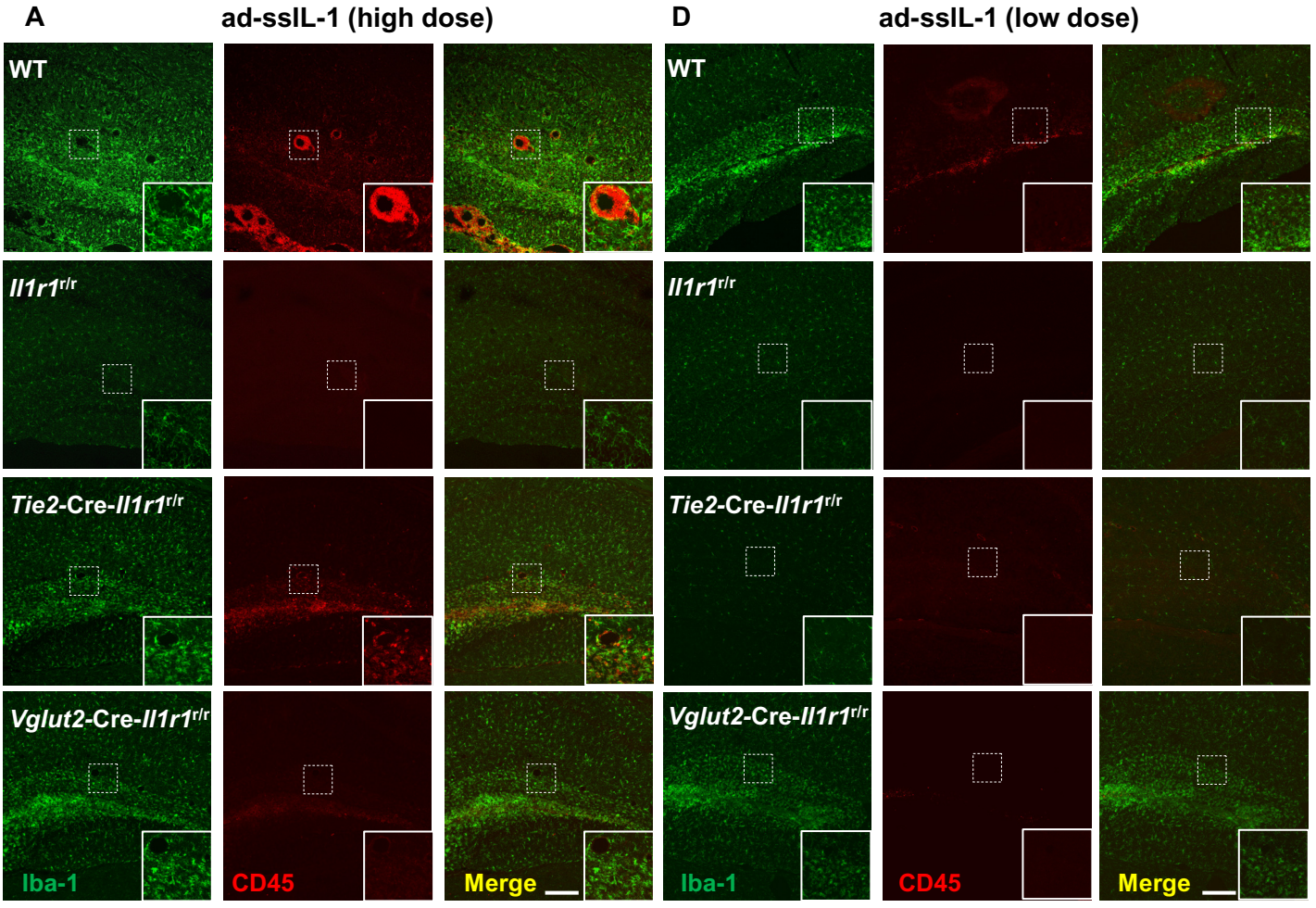
A
ad-sslL-1 (high dose)
D
ad-sslL-1 (low dose)
WT
Il1r1r/r
Tie2-Cre-Il1r1r/r
Vglut2-Cre-Il1r1r/r
Iba-1
CD45
Merge

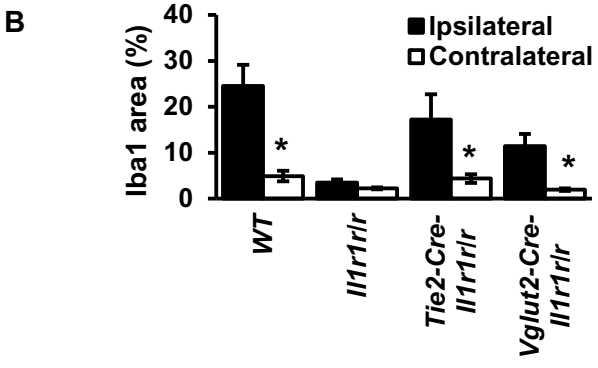
B
Iba1 area (%)
40
30
20
10
0
Ipsilateral
Contralateral
*
WT
Il1r1r/r
Tie2-Cre-Il1r1r/r
Vglut2-Cre-Il1r1r/r

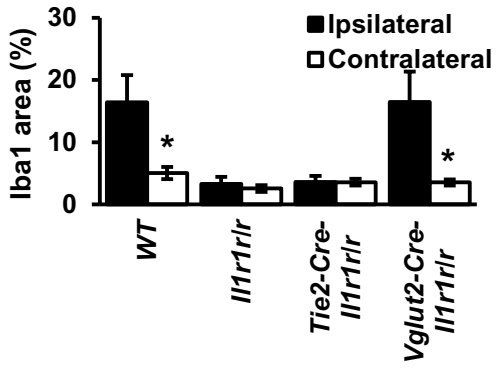
E
Iba1 area (%)
30
20
10
0
Ipsilateral
Contralateral
*
WT
Il1r1r/r
Tie2-Cre-Il1r1r/r
Vglut2-Cre-Il1r1r/r

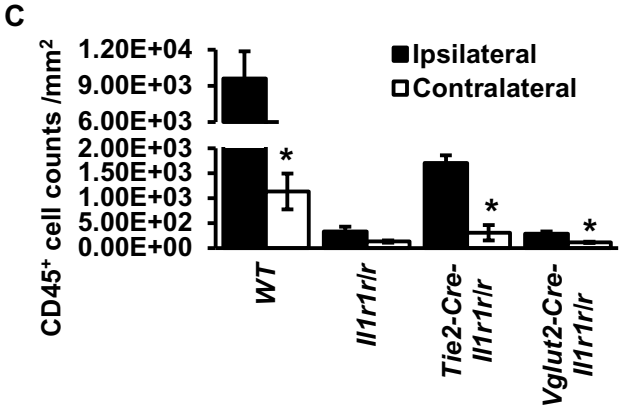
C
CD45+ cell counts /mm2
1.20E+04
9.00E+03
6.00E+03
2.00E+03
1.50E+03
1.00E+03
5.00E+02
0.00E+00
Ipsilateral
Contralateral
*
WT
Il1r1r/r
Tie2-Cre-Il1r1r/r
Vglut2-Cre-Il1r1r/r

Figure S3

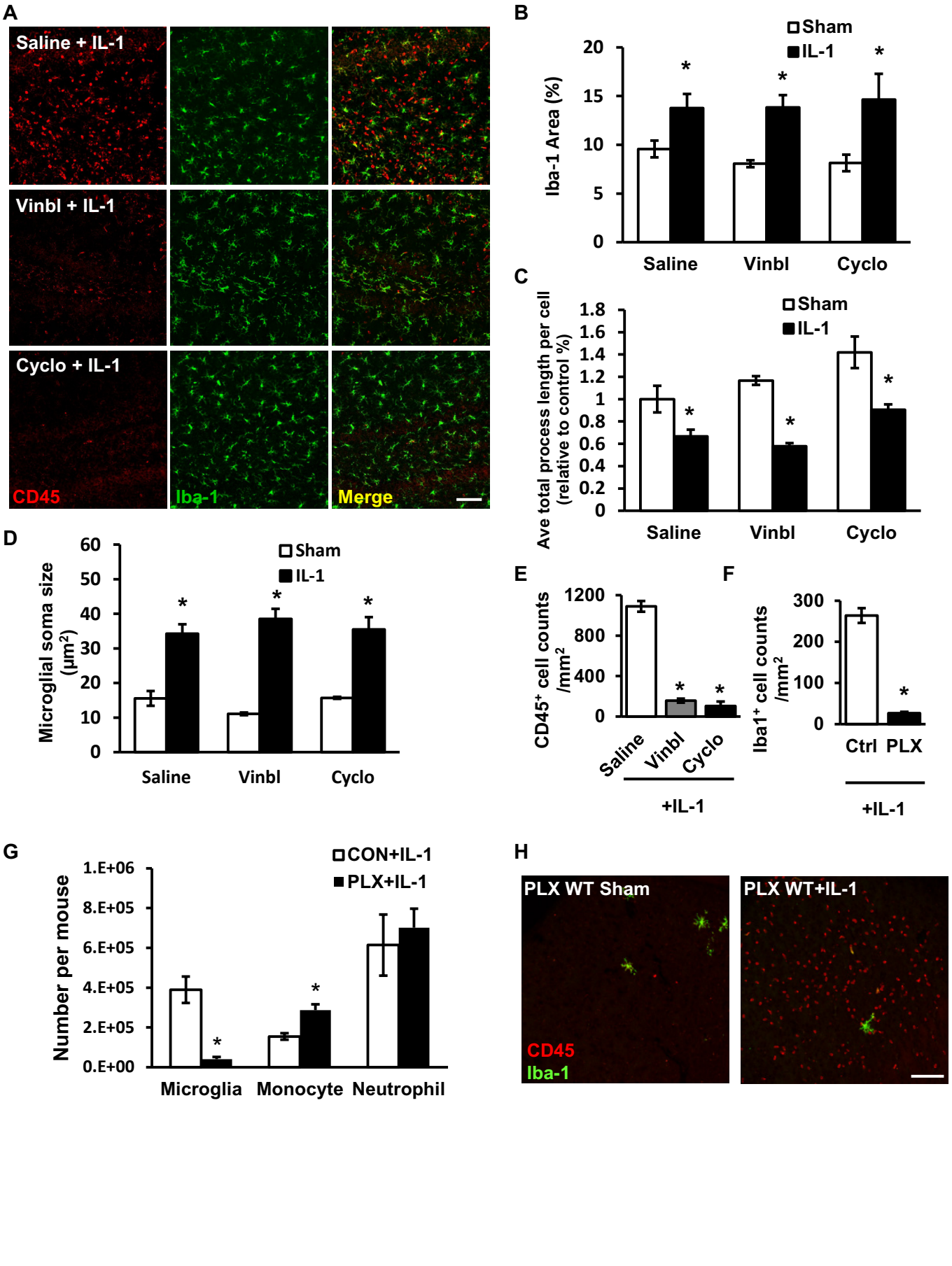
A
Saline + IL-1
Vinbl + IL-1
Cyclo + IL-1
CD45
Iba-1
Merge
B
Sham
IL-1
Iba-1 Area (%)
Saline
Vinbl
Cyclo
C
Ave total process length per cell (relative to control %)
D
Microglial soma size (μm²)
E
CD45⁺ cell counts /mm²
+IL-1
F
Iba1⁺ cell counts /mm²
Ctrl
PLX
G
CON+IL-1
PLX+IL-1
Number per mouse
Microglia
Monocyte
Neutrophil
H
PLX WT Sham
PLX WT+IL-1

Figure S4

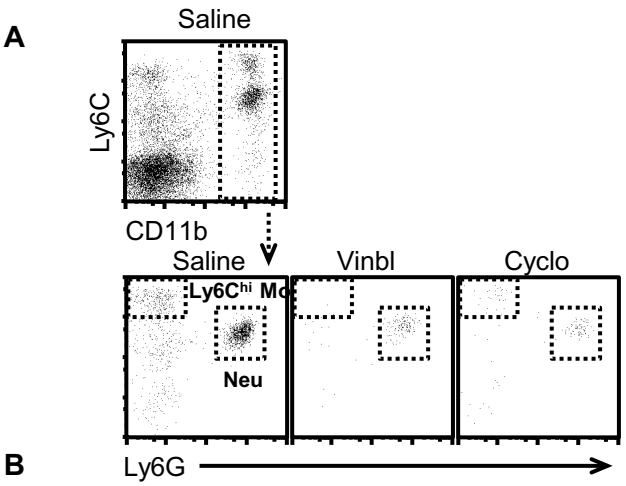

B

WBC population (Cells/mm³ ± SEM)	Total leukocytes	Neutrophils	Monocytes
Saline	10612 ± 1958	1118 ± 161	248 ± 52
Vinbl	3739 ± 259*	192 ± 65*	6 ± 1*
Cyclo	1265 ± 145*	121 ± 17*	42 ± 8*

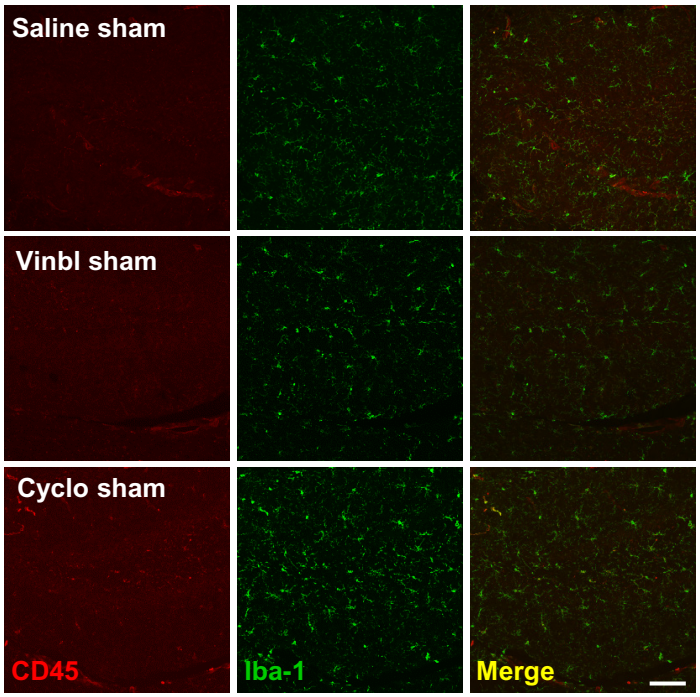

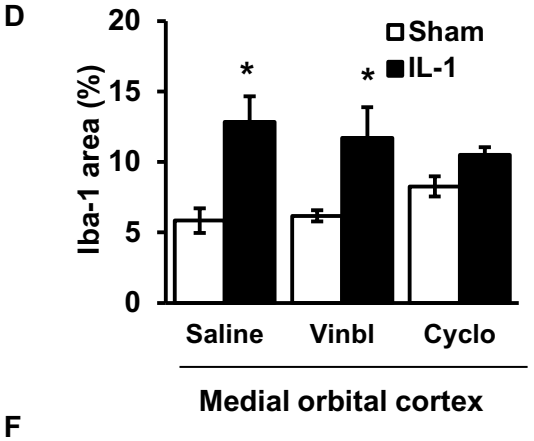

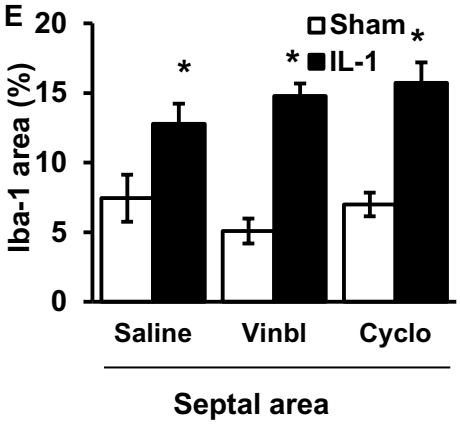

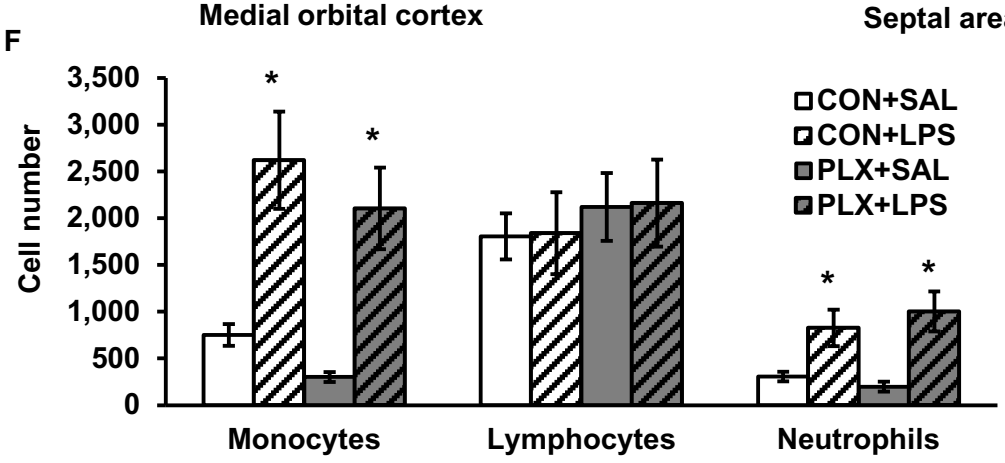

Figure S5

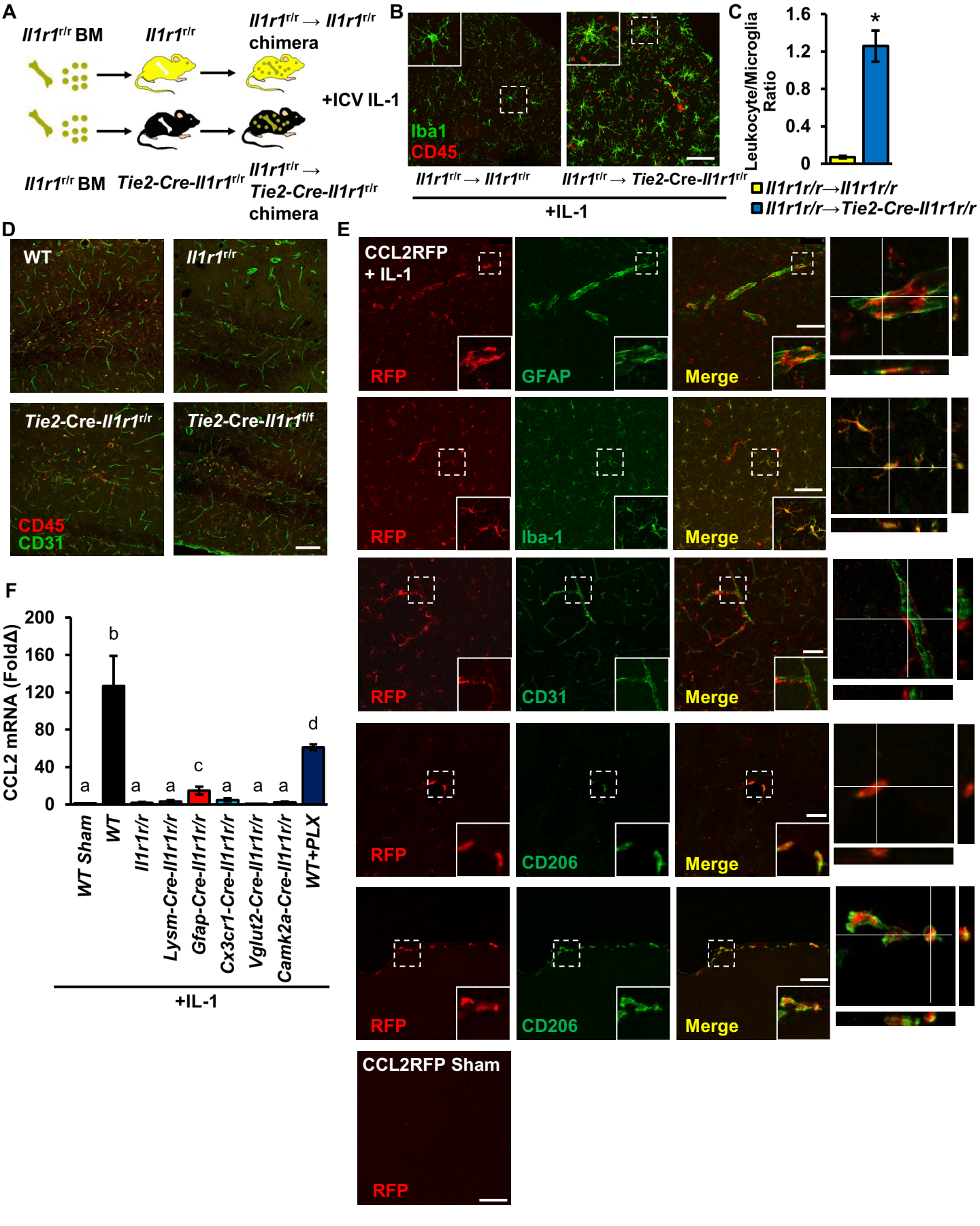
A
Il1r1r/r BM
Il1r1r/r
Il1r1r/r → Il1r1r/r chimera
+ICV IL-1
Il1r1r/r BM
Tie2-Cre-Il1r1r/r
Il1r1r/r → Tie2-Cre-Il1r1r/r chimera
B
Iba1
CD45
Il1r1r/r → Il1r1r/r
Il1r1r/r → Tie2-Cre-Il1r1r/r
+IL-1
C
Leukocyte/Microglia Ratio
1.6
1.2
0.8
0.4
0
*
Il1r1r/r→Il1r1r/r
Il1r1r/r→Tie2-Cre-Il1r1r/r
D
WT
Il1r1r/r
Tie2-Cre-Il1r1r/r
Tie2-Cre-Il1r1f/f
CD45
CD31
E
CCL2RFP + IL-1
RFP
GFAP
Merge
RFP
Iba-1
Merge
RFP
CD31
Merge
RFP
CD206
Merge
RFP
CD206
Merge
CCL2RFP Sham
RFP
F
CCL2 mRNA (FoldΔ)
200
160
120
80
40
0
a
b
a
a
c
a
a
a
d
WT Sham
WT
Il1r1r/r
Lysm-Cre-Il1r1r/r
Gfap-Cre-Il1r1r/r
Cx3cr1-Cre-Il1r1r/r
Vglut2-Cre-Il1r1r/r
Camk2a-Cre-Il1r1r/r
WT+PLX
+IL-1

Figure S6

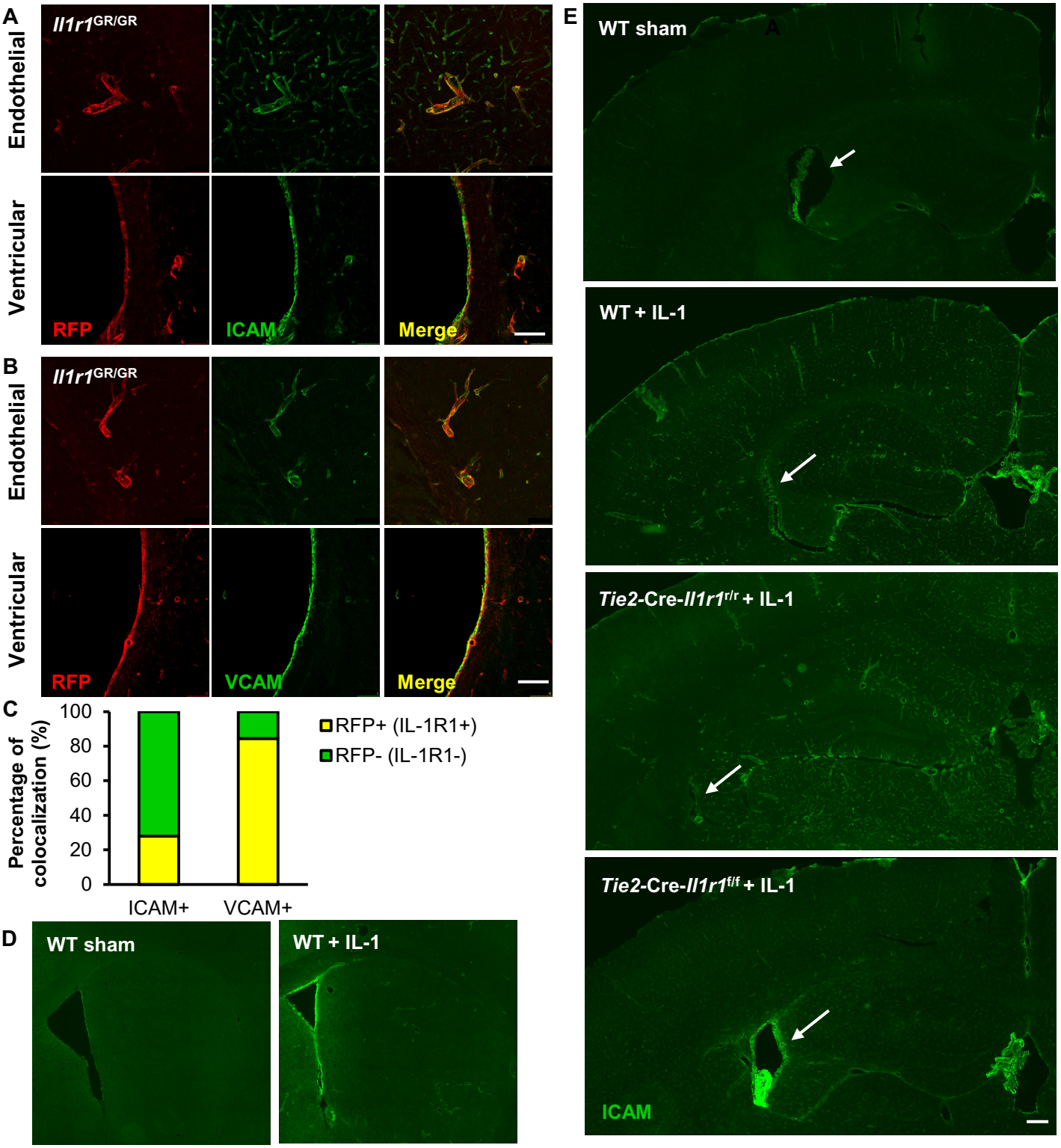
A
Endothelial
Ventricular
Il1r1GR/GR
RFP
ICAM
Merge
B
Endothelial
Ventricular
Il1r1GR/GR
RFP
VCAM
Merge
C
Percentage of colocalization (%)
100
80
60
40
20
0
ICAM+
VCAM+
RFP+ (IL-1R1+)
RFP- (IL-1R1-)
D
WT sham
WT + IL-1
Tie2-Cre-Il1r1r/r + IL-1
VCAM
Tie2-Cre-Il1r1f/f + IL-1
E
WT sham
WT + IL-1
Tie2-Cre-Il1r1r/r + IL-1
Tie2-Cre-Il1r1f/f + IL-1
ICAM

Figure S7

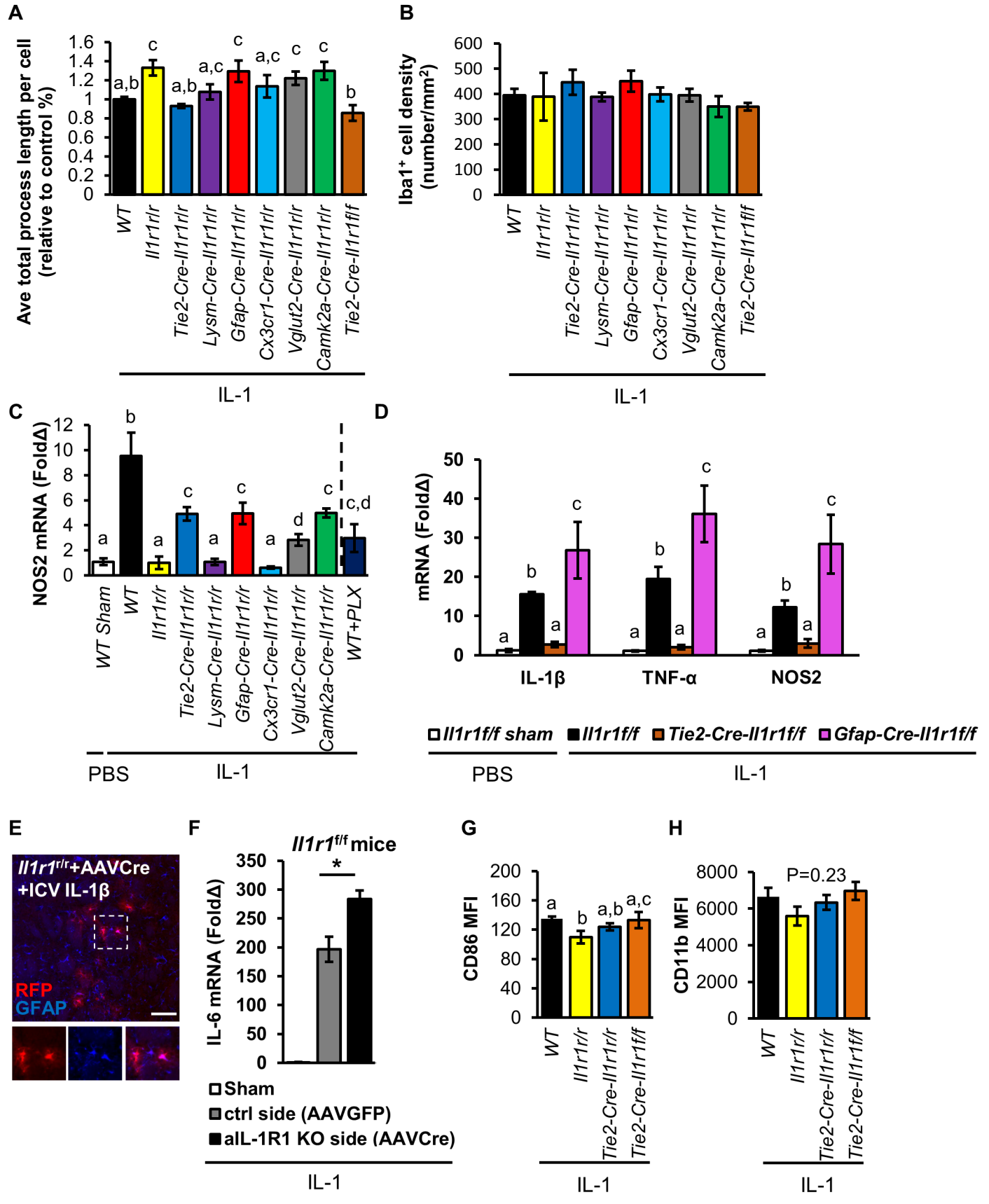
A
Ave total process length per cell (relative to control %)
1.6
1.4
1.2
1
0.8
0.6
0.4
0.2
0
a,b
c
a,b
a,c
c
a,c
c
c
b
WT
Il1r1r/r
Tie2-Cre-Il1r1r/r
Lysm-Cre-Il1r1r/r
Gfap-Cre-Il1r1r/r
Cx3cr1-Cre-Il1r1r/r
Vglut2-Cre-Il1r1r/r
Camk2a-Cre-Il1r1r/r
Tie2-Cre-Il1r1f/f
IL-1
B
Iba1+ cell density (number/mm2)
600
500
400
300
200
100
0
WT
Il1r1r/r
Tie2-Cre-Il1r1r/r
Lysm-Cre-Il1r1r/r
Gfap-Cre-Il1r1r/r
Cx3cr1-Cre-Il1r1r/r
Vglut2-Cre-Il1r1r/r
Camk2a-Cre-Il1r1r/r
Tie2-Cre-Il1r1f/f
IL-1
C
NOS2 mRNA (FoldΔ)
12
10
8
6
4
2
0
a
b
a
c
a
c
a
d
c
c,d
WT Sham
WT
Il1r1r/r
Tie2-Cre-Il1r1r/r
Lysm-Cre-Il1r1r/r
Gfap-Cre-Il1r1r/r
Cx3cr1-Cre-Il1r1r/r
Vglut2-Cre-Il1r1r/r
Camk2a-Cre-Il1r1r/r
WT+PLX
PBS
IL-1
D
mRNA (FoldΔ)
50
40
30
20
10
0
IL-1β
TNF-α
NOS2
Il1r1f/f sham
Il1r1f/f
Tie2-Cre-Il1r1f/f
Gfap-Cre-Il1r1f/f
PBS
IL-1
E
Il1r1r/r+AAVCre
+ICV IL-1β
RFP
GFAP
F
Il1r1f/f mice
IL-6 mRNA (FoldΔ)
350
300
250
200
150
100
50
0
*
Sham
ctrl side (AAVGFP)
aIL-1R1 KO side (AAVCre)
IL-1
G
CD86 MFI
200
160
120
80
40
0
a
b
a,b
a,c
WT
Il1r1r/r
Tie2-Cre-Il1r1r/r
Tie2-Cre-Il1r1f/f
IL-1
H
CD11b MFI
8000
6000
4000
2000
0
P=0.23
WT
Il1r1r/r
Tie2-Cre-Il1r1r/r
Tie2-Cre-Il1r1f/f
IL-1